

# Double enveloping worm gear modelling using CAD environment

Piotr POŁOWNIAK<sup>\*</sup>, Mariusz SOBOLAK, and Adam MARCINIEC

Rzeszow University of Technology, The Faculty of Mechanical Engineering and Aeronautics,  
al. Powstańców Warszawy 12, 35-959 Rzeszow, Poland

**Abstract.** This study describes the methodology for modelling a worm and worm wheel of a double enveloping worm gear with the use of a CAD system. An algorithm for generating a globoid helix is described. In addition, the methodology for modelling an hourglass worm thread with a straight axial tooth profile is presented. The shape of the hourglass worm tooth end with and without a trace modification is proposed. Moreover, a method for achieving a geometric modification of the tooth trace was developed. Next, the method for modelling the worm wheel teeth is described. A solid model of using a machining worm as a hob is applied. Owing to the limitations of a CAD system, which prevents the use of a direct machining simulation, an indirect modelling method is introduced. In the present study, different CAD techniques, both solid and surface, are applied. Knowledge of the correct modelling of the hourglass worm and worm wheel facilitates their generation and conducting various analyses, including a tooth contact analysis. CAD models are utilised to analyse the geometrical contact pattern in a CAD environment, to carry out FEM analysis, to manufacture real parts or to prototype models using the technique of rapid prototyping. They can be also used as master models for measurement, e.g. in optical technics.

**Key words:** globoid surface; CAD modelling; double enveloping worm gear; globoid helix; hybrid modelling; tooth trace modification.

## 1. Introduction

The double enveloping hourglass worm drive as reported by Dudas [1] and Crosner [2] was initially invented in 1765 by H. Hindley. At the beginning of the 20th century, Samuel I. Cone proposed that an hourglass worm be lathed using a lathe tool with a straight blade. A meshing worm gear is manufactured by an hourglass hob similar to an hourglass worm [3]. This type of drive is characterized by double lines and multi-tooth contact. It has greater transmission efficiency, a smaller size, and heavier load capacity in comparison with a cylindrical worm drive. Moreover, the forming condition of the lubricant layer between the teeth is quite good [4]. However, as a corresponding adverse effect, a globoid worm gear is sensitive to manufacturing and misalignment errors [5]. Owing to its advantages, this type of gear has rapidly become widely used. Chen et al. [6] reviewed the development history of worm drives and introduced their characteristics and applications. In addition, a systematic classification table of worm gears was proposed. Development trends and research hotspots of a worm drive were pointed out. The authors stated that a double-enveloping hourglass worm drive and a high-precision heavy-load worm drive will be the development priorities in the future.

Double enveloping worm drives have been the subject of research conducted by numerous scientists. Mathematical modelling and analyses of gears, the introduction of modifications, surface analyses, the development of new types of globoid worm gears, and manufacturing methods still continue.

Litvin [4] presented a simplified geometrical analysis of a TA worm drive. The helicoidal surface of a worm was not considered in the analysis. The investigation was divided into unmodified and modified drives and relevant modification parameters such as the centre distance and velocity ratio. Simon [7, 8] proposed a new type of double-enveloping worm gear drive. The gear tooth surface of the worm gearing is shaped by a flying tool whose cutting edge is identical to the profile of the entering edge of the worms. Simon developed a method for the determination of the load distribution in a double enveloping worm gear [9]. The author also proposed a newly modified type of such drive [10]. In addition, Zhao, and Zhang [11] conducted a curvature analysis for a helicoidal surface of a modified TA worm. They disclosed in their study [12] the core role and fundamental position of the normal vector of the instantaneous contact line based on the meshing theory for line-conjugate tooth surfaces. Next, Zhao [13] conducted a meshing analysis for a TA worm drive and confirmed that two contact lines exist simultaneously. The author proposed improving the meshing performance further by dislodging the constant contact line through modification. The findings of the study conducted by Huai et al. [14] show that a variable height modification can remove the constant contact line from the tooth surface of the worm wheel and that the global meshing performance of a variable height-modified TA worm drive is considerably improved. Zhao [15] suggested a methodology for counting the addendum thickness of the edge tooth for a TA worm and attained an analytical solution regarding the top thickness of the edge tooth. Zhao et al. [16] also established a meshing geometry of a modified globoid worm drive. The modification parameters included the centre distance, the transmission ratio, and the cutter frame height while machining the worm. A full mathematical description of the tooth flank surface of the globoid

\*e-mail: ppolowniak@prz.edu.pl

Manuscript submitted 2020-09-21, revised 2020-11-24, initially accepted for publication 2021-01-04, published in April 2021

worm and worm wheel was presented by Polowniak and Sobolak [17], who established the axial section of the worm as a straight line, where the worm wheel was generated using a hob cutter, which is identical to a TA worm. Wen, Xu, and Tang [18] described a research method of a new modification principle for toroidal worm gearing. Chen et al. [19] presented a novel hourglass worm drive, called an involute gear meshing with a planar enveloping hourglass worm drive. They studied the theory of a tooth contact analysis of an hourglass worm drive, which was developed through numerical and finite element analyses. He, Shi, and Yu [20] established a modification for a planar double-enveloping hourglass worm gear drive to eliminate the phenomenon of a crossed contact line. The modification is achieved by changing the partial process parameters of the first envelope, e.g. by changing the centre distance, transmission ratio, and relative position.

Methods for the mathematical modelling of the worm wheel teeth are complex. Xu and co-authors [21] proposed a direct digital modelling method for a worm gear drive, which is based on the practical manufacturing process. The concept of worm wheel tooth generation using the different axial section profiles of the worm representing the hob cutting edges was introduced by Mohan and Shunmugam [22]. In their study, the generation of a worm wheel tooth flank by the fly cutter representing the end tooth of a hob was presented. Chen and Tsay [23] studied an hourglass worm gear composed of a ZN-type hourglass worm generated by straight-edged blade cutters and a worm wheel generated by worm-type hourglass hob cutters.

Subjects of investigation associated with the geometry of an hourglass worm hob are still under consideration. Rui et al. [24] presented a method for designing the land surfaces of a hob with spiral rake faces to increase the service life of the hob. Yang and co-authors [25] proposed a method for generating a spiral flute of a planar double enveloping hourglass worm gear hob based on the curved surface generating theory and the hourglass worm forming principle. The machining of the spiral flutes was simulated using a virtual manufacturing system, and the results verify the correctness of the method. Rui et al. [26] put forward a design and generation method of a dual-cone double-enveloping hourglass worm gear hob for grinding the relief surfaces in which the land widths and relief angles are precisely machined.

Aspects of the manufacturing process of worm gear sets have been the subjects of investigation of numerous researchers. Zhong et al. [27] proposed a high-precision and efficient machining method using a conical cutter of a plane double enveloping hourglass worm. In their study, Lagutin and co-workers [28] presented a technique for the geometrical design of globoid gears modified by increasing the machine-tool centre distance and gear ratio while cutting the worm with respect to the same parameters of the worm gear. Tooth machining using fly-blades with two or four cutters was described. Sutyagin et al. [29] developed a method to increase the efficiency of the tooth cutting of a globoid worm. They proposed the use of rotary machining through a multi-cutter with an involute profile. Dong and co-workers [30] presented a new rough turning method based on a discretization of the spiral surfaces of the

toroidal worm. Sun et al. [31] introduced a conceptual method for precise grinding of a single enveloping TI worm. Dudás [5] suggested a solution for producing quasi-globoid worm gearings using a normal lathe with a tilted worm holder to cut the threads, and the worm wheel is then generated through this quasi-globoid worm.

An investigation into a CAD modelling method for enveloping the surface parts including a double-enveloping surface is still ongoing. Liu et al. [32] introduced a novel CNC machining method for an enveloping surface based on the enveloping characteristic, namely the contact lines. This method was conducted for a double-enveloping surface. Liu et al. [33] proposed the use of digitization modelling and a CNC machining method for a cone-generated double-enveloping worm drive. Lu and co-workers [34] developed a digital CAD modelling method and CNC machining for enveloping the surface parts. Kheyfets [35, 36] presented in a demonstrative way, through drawing schemes and short descriptions, a concept of CAD modelling of a worm and worm wheel tooth surface.

This study aims to present a modelling methodology of the worm and worm wheel of a globoid worm gear in a CAD environment. The knowledge of the correct modelling of the hourglass worm and worm wheel allows their generation and helps in conducting various analyses including a TCA analysis.

The investigation of the double enveloping worm gear is mainly focused on the mathematical meshing analysis or manufacturing aspects. Furthermore, the meshing analyses are carried out in the range of effective worm length. A CAD model of a globoid worm considers the whole thread length, which allows a complete analysis of the correctness of meshing. In this paper, the formation of a worm tooth beyond this range for both the active and passive tooth flank is described. The first step of the proposed solution is to cut the tooth where the effective worm length ends. The second step is to modify the tooth trace. It is supposed that a globoid worm with a tooth trace modification at the ends of the thread should be characterised by a more favourable stress distribution during the entry into meshing and greater rigidity of the beginning of the thread. It needs to be investigated in the future.

The presented methodology for modelling the worm and worm wheel of a globoid worm gear in a CAD environment can be particularly useful for engineers designing such gears. They are usually fluent users of CAD systems and can build the gear model themselves. CAD models are applied in the analysis of the geometrical contact pattern in a CAD environment [37], in carrying out the FEM analysis [38–40], manufacturing real parts, or prototyping models through the technique of rapid prototyping [41, 42]. They can be also used as reference models for measurement.

## 2. Modelling a worm of globoid worm gear

In the process of modelling, aspects such as the transmission ratio (the number of worms and worm gear teeth), the module, the centre distance, the tooth flank angle, the pitch diameter of the worm, and the worm gear are determined. The standard

in [43] presents formulas for calculating the general gearset proportions for the globoid worm gearing assembled with axes at a  $90^\circ$  angle. There are also other standards available that provide incomplete guidelines for the design of a double enveloping worm gear [44–47]. Adopting the basic parameters facilitates the creation of a worm profile in the axial section. Fig. 1 shows the nominal reference profile of the worm tooth space in such a section. Depending on whether a working worm or a worm applied as a geometrical tool for the modelling of a worm wheel are modelled using a direct machining simulation in a CAD environment, the profile is modified using the appropriate clearance.

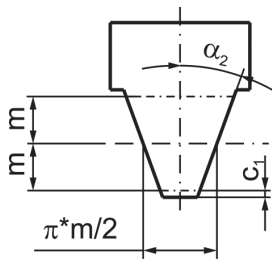


Fig. 1. Nominal axial reference profile of the tool for generating a tooth space profile of a globoid worm:  $m$ , module;  $\alpha_2$ , tool profile angle; and  $c_1$ , tip clearance

In a worm with a rectilinear tooth profile, the outline of the tool coincides with the profile of the worm wheel tooth space in the central plane, as well as with the axial profile of the worm tooth in the case of a zero circumferential backlash.

Fig. 2 shows the analysis and method for creating the central section of the wheel and the axial section of the worm. Based on the tooth thickness used in the globoid worm gearbox, the structural materials are usually designed at a proportion of ap-

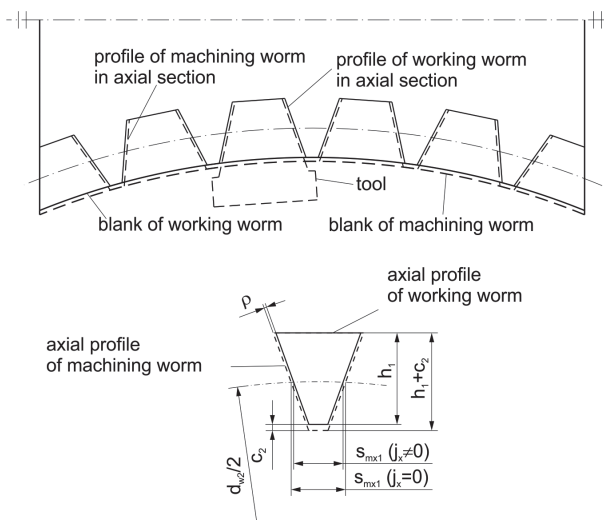


Fig. 2. Principle of creating a globoid worm gear in the axial section:  $\rho$ , the angle between the axial profile of machining worm and working worm;  $s_{mx1}(j_x = 0)$ , tooth thickness of the machining worm;  $s_{mx1}(j_x \neq 0)$ , tooth thickness of the working worm;  $j_x$ , backlash;  $d_{w2}$ , the pitch diameter of the worm wheel;  $h_1$ , tooth height of the working worm;  $h_1 + c_2$ , tooth height of the machining worm;  $c_2$ , tip clearance

proximately 0.55 of the circular pitch of the worm gear and approximately 0.45 for the worm. For this purpose, the nominal axial outline of the tool can be modified [43]. The outline of the tool is copied in a circular pattern around the centre of the worm wheel. Thus, the centre of the worm wheel is obtained. Creating a worm outline in the axial section requires determining the effective worm thread length  $b_{1eff}$  (or the angle of the active worm range  $\Omega$  defined in relation to the centre of the worm wheel). The specified axial section of the worm will be characterised by zero circumferential clearance in the meshing of the gear. The model based on the above tooth outline in the axial section will be applied if the worm model is used as the geometry of the worm wheel modelling (the so-called machining worm). The thickness of the worm wheel tooth space will be the same as the thickness of the worm tooth. When modelling a working worm, it is necessary to consider the tip clearance  $c_2$  and the circumferential backlash expressed by the angle  $\rho$  (Fig. 2). For such a geometric analysis, a sketcher workbench available in any CAD system is used.

After defining the axial section and the effective length of the worm, the coordinates of the four characteristic tooth profile points should be determined (Fig. 3) [17]. These are points A, B, C, and D which are the vertices of the adopted straight-line profile of the globoid worm, and are described by the following vectors:

$$\vec{r}_A^{(1)} = \begin{bmatrix} x_{1A} \\ y_{1A} \\ z_{1A} \\ 1 \end{bmatrix}, \quad \vec{r}_B^{(1)} = \begin{bmatrix} x_{1B} \\ y_{1B} \\ z_{1B} \\ 1 \end{bmatrix}, \quad \vec{r}_C^{(1)} = \begin{bmatrix} x_{1C} \\ y_{1C} \\ z_{1C} \\ 1 \end{bmatrix}, \quad \vec{r}_D^{(1)} = \begin{bmatrix} x_{1D} \\ y_{1D} \\ z_{1D} \\ 1 \end{bmatrix}. \quad (1)$$

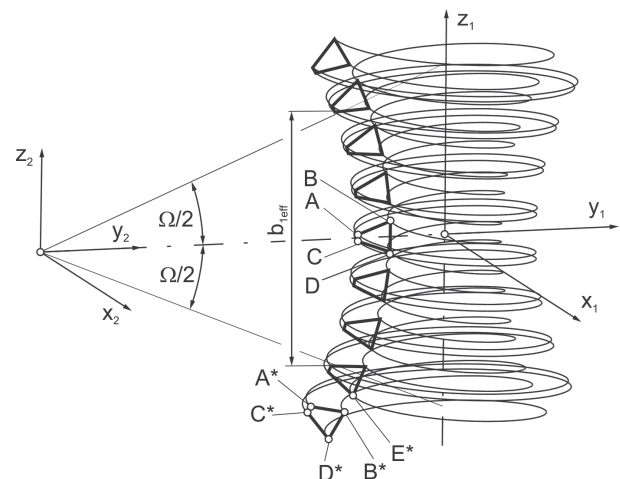


Fig. 3. Principle of globoid worm modelling

The basis for modelling a globoid worm is a helix, which is created as a spline curve based on a set of points. This set is generated in an external program (MS Excel, MATLAB) and imported into the CAD environment. Alternatively, helix can be described mathematically by parametric equations without using transformation matrices [48].

The coordinates of a given point, A, B, C, and D, are inserted into the formula for a globoid helix. Obtaining the analytic equation of a globoid helix is based on the determination of successive positions of any point (P) on the worm tooth (Fig. 4).

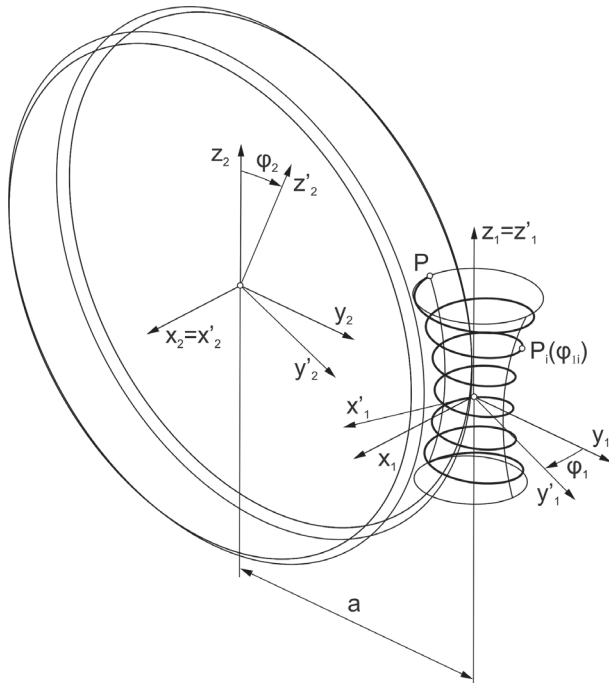


Fig. 4. The coordinate system of globoid worm gear:  $P$  – any point on the tooth flank of the worm in the plane  $y_1z_1$ ;  $P_i(\varphi_{1i})$  – position of point  $P$  after transformation of the system  $x'_1y'_1z'_1$  by an angle  $\varphi_{1i}$ ; and  $a$  – centre distance between the worm and worm wheel

Figure 4 shows the two stationary coordinate systems  $S_1(x_1y_1z_1)$  and  $S_2(x_2y_2z_2)$  connected with the worm and worm wheel, respectively. These systems can be handled as systems associated with housing. The moveable coordinate systems  $S'_1(x'_1y'_1z'_1)$  of the worm and  $S'_2(x'_2y'_2z'_2)$  of the worm wheel were introduced. The worm rotates around the  $z'_1$  axis by the angle  $\varphi_1$  opposite to the trigonometric direction. Then, the worm wheel rotates around the  $x'_2$  axis with the  $\varphi_2$  angle, as well as the opposite to the trigonometric direction (in the case of using a left-hand thread worm).  $\varphi_1$  is a geometric parameter, whereas  $\varphi_2$  is an auxiliary parameter. There is a relation between  $\varphi_1$  and  $\varphi_2$  that results from the following transmission ratio:

$$i = \frac{\varphi_2}{\varphi_1}. \quad (2)$$

The centres of the coordinate systems were positioned away from each other by the value  $a$ .

The description of the globoid helix is made by using homogeneous matrices of transformation. Matrices are used to represent transformations between systems. The matrices  $M_{xy}$  concern transformations between systems.  $M_{xy}$  is a homogeneous transformation matrix from the system  $y$  to  $x$ . For  $x$  and  $y$ , the appropriate index related to the coordinate system number is inserted.

It was assumed that point  $P$  lies on the tooth side of the worm located in the plane  $y_1z_1$ . The vector determines the point:

$$\bar{r}_P^{(1)} = \begin{bmatrix} x_1 \\ y_1 \\ z_1 \\ 1 \end{bmatrix}. \quad (3)$$

A parametric equation of the globoid helix is shown as the vector  $\bar{r}_P^{(1')}$ . Homogenous transformation matrices between particular coordinate systems were used:

$$\bar{r}_P^{(1')} = M_{1'1} \cdot M_{12} \cdot M_{2'2} \cdot M_{21} \cdot \bar{r}_P^{(1)}. \quad (4)$$

The developed form of vector  $\bar{r}_P^{(1')}$  is presented as follows [17]:

$$\bar{r}_P^{(1')} = \begin{bmatrix} x_1 \cdot \cos(\varphi_1) - a \cdot \sin(\varphi_1) + a \cdot \cos(\varphi_2) \cdot \\ \cdot \sin(\varphi_1) + y_1 \cdot \cos(\varphi_2) \cdot \sin(\varphi_1) - \\ - z_1 \cdot \sin(\varphi_2) \cdot \sin(\varphi_1) \\ - x_1 \cdot \sin(\varphi_1) - a \cdot \cos(\varphi_1) + a \cdot \cos(\varphi_1) \cdot \\ \cdot \cos(\varphi_2) + y_1 \cdot \cos(\varphi_2) \cdot \cos(\varphi_1) - \\ - z_1 \cdot \sin(\varphi_2) \cdot \cos(\varphi_1) \\ a \cdot \sin(\varphi_2) + y_1 \cdot \sin(\varphi_2) + z_1 \cdot \cos(\varphi_2) \\ 1 \end{bmatrix}. \quad (5)$$

The range of the worm tooth should be determined using the parameter  $\varphi_{1p}$ . The parameter  $\varphi_{1p}$  changes from the initial value  $\varphi_{1k}$  with a step of  $\Delta\varphi_1$ . The number of points depends on  $\Delta\varphi_1$ , and thus the accuracy of the spline of the globoid helix will approximate.

Based on the algorithm, sets of points representing individual globoid worm helices originating from points A, B, C, and D were obtained. These points were introduced into a CAD environment (Fig. 5a). In this case, the CATIA V5R21 system was used. Spline curves approximating globoid helices were developed on the appropriate sets of points (Fig. 5b). The profiles

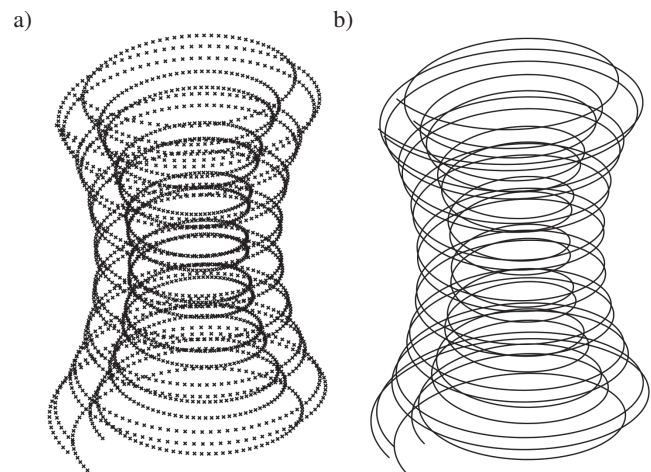


Fig. 5. Globoid helices represented as (a) sets of points and (b) splines developed on sets of points

were created at one end of a globoid worm (Fig. 3). Sections  $A^*B^*$  and  $C^*D^*$  are the profiles of the worm tooth in the axial section, and section  $A^*C^*$  closes the top land. Owing to the modelling method applied, an additional helix line was generated from point D ending at point  $E^*$  (the range of this helix is  $2\pi$  smaller compared to the helix ending at point  $D^*$ ). Section  $B^*E^*$  closes the bottom land (Fig. 3).

Worm tooth modelling can proceed using the profile lines and helices which are the swept surface definition. To consider the changes in the surface curvatures, the swept profile should follow two guide curves. For each surface, the flank, top, and bottom are created through separate operations (*Sweep-Explicit*) (Fig. 6a). It is also possible to make a globoid surface by developing the surface between two guide curves (*Sweep-Line*) (Fig. 6b).

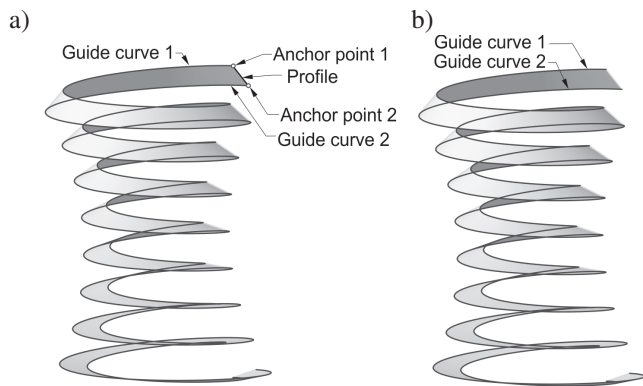


Fig. 6. Creation of a globoid surface by (a) sweeping a profile through guide curves and b) developing a surface between guide curves

Owing to the changes in the curvatures in two directions, it is not possible to create a globoid worm tooth by extruding the profile along one guide curve (Fig. 7), as in the case of a cylindrical worm.

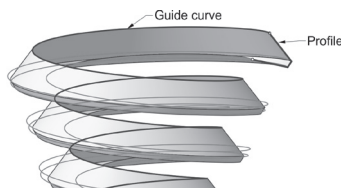


Fig. 7. Development of worm thread along one guide curve; a fragment of the model with globoid helices

When the surface of the tooth flank is modelled by a sweep operation (Fig. 6a, 6b), a slight distortion of the surface occurs. This is because the output profile is projected onto a plane normal to one of the guide curves (Fig. 8). Thus, the axial section of the created surface is not rectilinear.

In Fig. 9, surfaces of the globoid worm created through sweep operations are shown.

Another way of modelling is to make the surface of the worm multi-sectional. In this case, the profiles should be created between the respective points of the globoid helices as axial sections of the worm (Fig. 10).

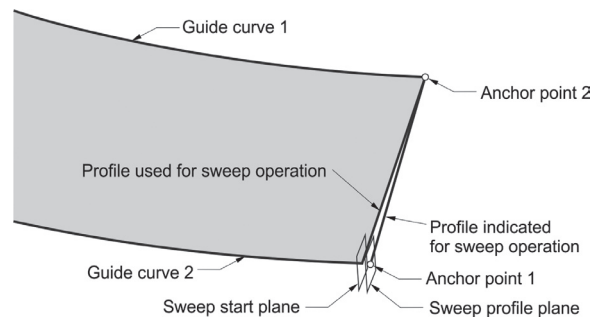


Fig. 8. Cause of error when the globoid surface is modelled using a sweep operation (fragment of a globoid surface)

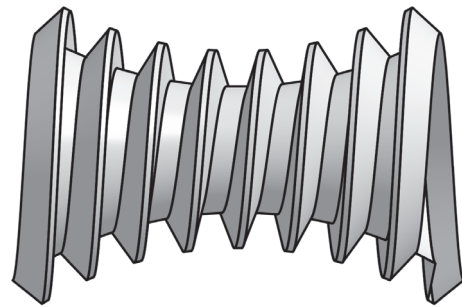


Fig. 9. Surface of a globoid worm

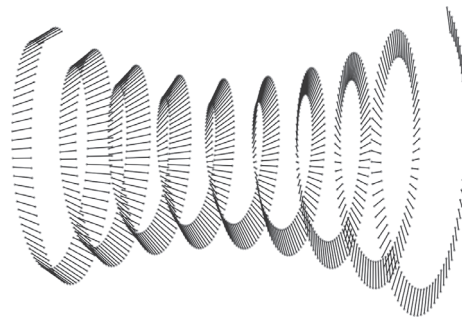


Fig. 10. Created profiles between the corresponding points of globoid helices for one tooth flank

Modern CAD systems allow the writing of macro programs. In modelling a globoid surface, a macro program (Fig. 11) can be written to connect the relevant points of the globoid helices in the profiles. These represent the axial tooth profiles of the globoid worm. The globoid surface was developed as a multi-sectional surface (Fig. 12).

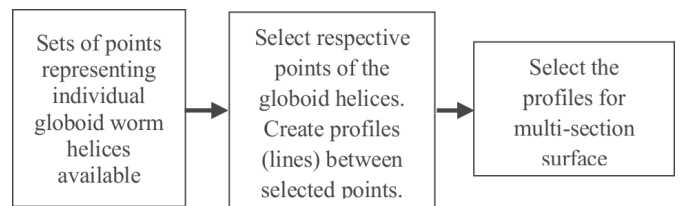


Fig. 11. Flowchart of a macro program connecting the relevant points of the globoid helices in the profiles and then on the surface

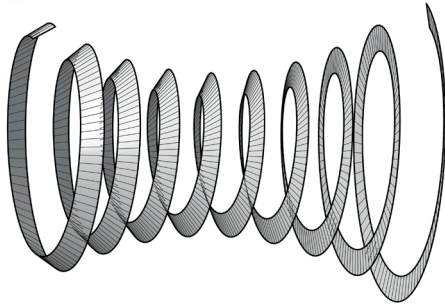


Fig. 12. A globoid surface created using a multi-section surface method

The top and bottomland surfaces of a thread can be modelled using a sweep operation (Fig. 13) or a multi-sectional surface method.

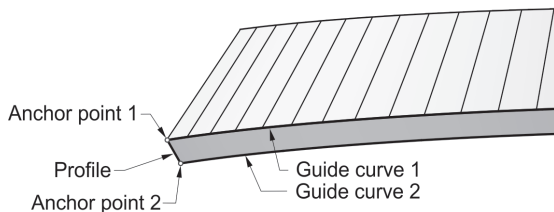


Fig. 13. A fragment of a surface made using a multi-sectional surface method (tooth flank) and a sweep operation using profile and guide curves (top land)

The globoid worm created using the multi-section surface method has a rectilinear axial section, which is correct.

By modelling the worm surfaces, the effective worm length was assumed. A worm tooth beyond this range can be formed in two ways. The first solution is to cut the tooth, where the effective worm length ends. The second proposition is to modify the tooth trace.

In the case of the first solution, two cutting planes should be introduced into the axial plane (Fig. 14). The position of the axial planes is determined based on the effective worm length  $b_{1eff}$  [43]. These planes cut the top land, flank, and bottomland surfaces. Additional surfaces filling the ends of the worm tooth were applied. All created surfaces were then joined and closed into a solid (Fig. 15).

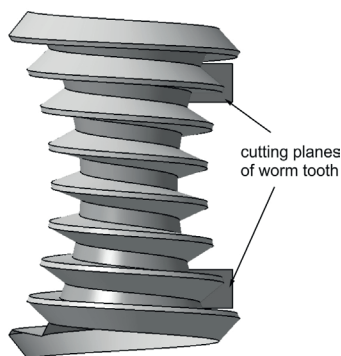


Fig. 14. Surfaces of globoid working worm with cutting planes

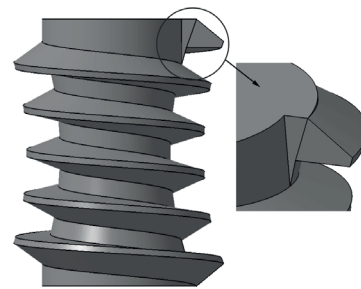


Fig. 15. Model of globoid working worm with cut tooth ends

A globoid worm with such a formed tooth may result in the occurrence of concentrated stress at the beginning of the tooth during entry into the meshing.

The tooth ending of the globoid worm may result from the shape of the worm blank. Then, the tooth ends on its conical surfaces. When the conical surfaces of a worm blank are located near the ends of the effective worm thread length, a thinned tooth will be formed and the contact region in this fragment will have the shape of a wedge (Fig. 16).

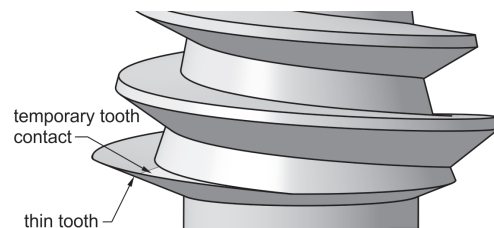


Fig. 16. Model of a globoid worm and contact region at the entrance of the mesh

The worm thread should be in the mesh within the entire working depth of the tooth and within the limit of the effective thread length of the worm specified in the model by  $\varphi_{1p}$  and  $\varphi_{1k}$ . The end of the thread on both sides of the tooth is subject to modification, i.e. active and passive tooth flanks. The boundary of the modified and unmodified surfaces is the parameter  $\varphi_{1p}$  for one side and  $\varphi_{1k}$  for the other.

The stages of the modelling of one thread end are shown, whereas the other end is modelled analogously. The globoid worm helices used to model the flank surface of a tooth without a trace modification are created based on Eq. (5). To create a flank surface with a tooth trace modification, additional globoid worm helices should be determined, starting at the ends of the helical curves made without modification. The coordinates of the points  $A^I$ ,  $B^I$  and  $C^I$ ,  $D^I$  (Fig. 17) are determined based on Eq. (5) and the positional vectors to particular points  $A$ ,  $B$  and  $C$ ,  $D$  (1). The points  $A^I$ ,  $B^I$  and  $C^I$ ,  $D^I$  determine the beginning of the modification:

$$\begin{aligned} \vec{r}_{A^I}^{(1')}(\varphi_1 = \varphi_{1p}) &= M_{1'1}^* \cdot \vec{r}_A^{(1)}, \\ \vec{r}_{B^I}^{(1')}(\varphi_1 = \varphi_{1p}) &= M_{1'1}^* \cdot \vec{r}_B^{(1)}, \end{aligned} \quad (6)$$

$$\begin{aligned}\bar{r}_{C^I}^{(1')}(\varphi_1=\varphi_{1p}) &= M_{1'1}^* \cdot \bar{r}_C^{(1)}, \\ \bar{r}_{D^I}^{(1')}(\varphi_1=\varphi_{1p}) &= M_{1'1}^* \cdot \bar{r}_D^{(1)},\end{aligned}\quad (7)$$

where

$$M_{1'1}^* = M_{1'1} \cdot M_{12} \cdot M_{2'2} \cdot M_{21}. \quad (8)$$

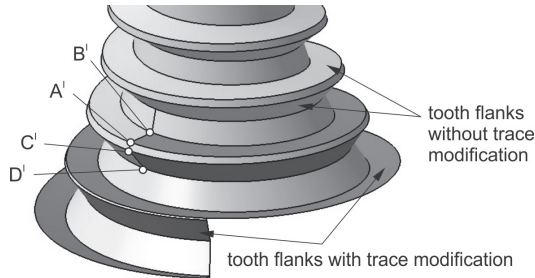


Fig. 17. Worm tooth flanks made with and without tooth trace modification

In matrix  $M_{1'1}^*$  of Eqs. (6) and (7) for  $\varphi_1$ ,  $\varphi_{1p}$  is inserted, and  $\varphi_2 = \varphi_{1p} \cdot i$ . In the case of a globoid worm, the tooth trace modification involves changing the pitch angle, which can be obtained by considering the following expression:

$$\varphi_2 = T \cdot i \cdot \varphi_1, \quad (9)$$

where  $T > 1$  in the case of an active flank and  $T < 1$  in the case of a passive flank.

Vectors generated from Eqs. (6) and (7) should be inserted into the following expression:

$$\begin{aligned}\bar{r}_{p^I}^{(1')} &= M_{1'1}(\varphi_1=\varphi_{1p}) \cdot M_{1'1} \cdot M_{12} \cdot M_{2'2} \cdot \\ &\cdot M_{21} \cdot M_{11'}(\varphi_1=\varphi_{1p}) \cdot \bar{r}_{i^I}^{(1')}(\varphi_1=\varphi_{1p}),\end{aligned}\quad (10)$$

where  $\bar{r}_{i^I}^{(1')}(\varphi_1=\varphi_{1p})$  is the vector of the selected points from Eqs. (6) and (7).

New globoid worm helices are obtained starting at the ends of the un-modified helices. Eq. (9) should be considered in matrix  $M_{2'2}$  in Eq. (10). The main parameter is  $\varphi_1$ , which changes from  $\varphi_{1p}$  to  $\varphi_{1p} - \varphi_{1w}$  with a discretization step of  $d\varphi_1$  ( $\varphi_{1w}$  is the value at which the modelled worm thread will be outside the worm blank). Based on Eq. (10), sets of points representing globoid helices originating from points  $A^I$ ,  $B^I$  and  $C^I$ ,  $D^I$  are obtained. These points were introduced into the CAD environment. Sections were created between the corresponding points of the globoid helices. The modelling of a globoid worm with a tooth trace modification at the end of the thread requires the use of a multi-section surface method in a CAD environment. Then, there will be no gaps between the surfaces of the given tooth flank, which will occur with the surface modelling method when using a sweep operation. The surfaces of the tooth flank with and without modification should be joined. The entire flank of the tooth was created. After modelling the missing surfaces at the end of the thread (top and bottom land) and

joining all surfaces made, the surfaces of the worm tooth were obtained (Fig. 17).

The next step is the execution of conical surfaces based on the contour of the blank. These surfaces are used to cut both sides of the worm model (Fig. 18), shaping the ends of the thread. The cylindrical parts of the worm are then modelled. The last stage is a transformation of the closed surfaces into a solid (Fig. 19).

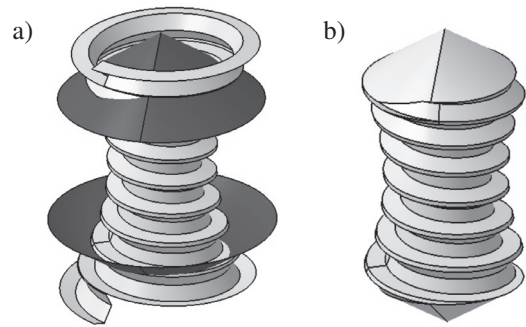


Fig. 18. (a) Creation of conical surfaces and (b) cutting of the worm using these surfaces

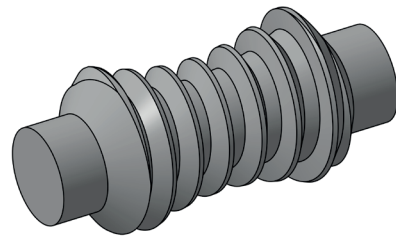


Fig. 19. Model of globoid worm

A globoid worm with a tooth trace modification at the ends of the thread should be characterised by more favourable stress distribution during the entry into the meshing and greater rigidity at the beginning of the thread. The CAD model of the globoid worm considers the whole thread length, which facilitates a complete analysis of the correctness of meshing.

### 3. Modelling of a worm wheel

The worm wheels of globoid gears can be machined in an enveloping or shaped manner. A profiling of the teeth is extremely labour-intensive. In the case of an envelope processing, an hourglass hob is similar to an hourglass worm. In the worm geometry (the so-called machining worm) used for modelling the worm wheel, appropriate clearances (tip clearance and circumferential backlash) should be provided (Fig. 2), increasing the thread length of the machining worm in relation to the working worm. The tool model is made based on a worm modelling methodology with a cut thread. The model of the machining worm is shown in Fig. 20. In actual machining, the tooth surface of the worm wheel is shaped by a definite number of cutting edges of the hob cutter. A modelled tool can be imagined as a cutter in which an infinite number of cutting edges were made.

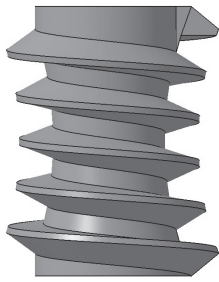


Fig. 20. Globoid machining worm

After modelling the tool, a workpiece model should be created. The workpiece is modelled solidly and partially corresponds to the blank before processing. In the CAD system, the tool and blank model must be set correctly within the space so that the axial plane of the worm is in coincidence with the central plane of the blank and their axes are located at an angle of  $90^\circ$  and spaced apart by the nominal value of the centre distance. In the following, coordinate systems were assigned successively as  $x_1y_1z_1$  for the machining worm and as  $x_2y_2z_2$  for the worm wheel blank. The rotation of the tool describes the angle  $\varphi'_1$ , and the blank describes the angle  $\varphi'_2$  (Fig. 21). A fixed  $xyz$  system is also introduced, which can be treated as a system associated with the machine body. During the machining, the object and tool rotate with movements resulting from the kinematics of the gear generation and are dependent on the gear machining ratio, which is compatible with the transmission ratio.

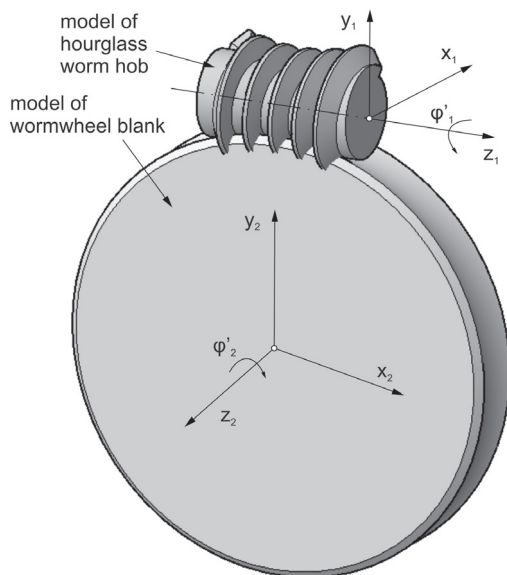


Fig. 21. The principle of worm wheel modelling:  $x_1y_1z_1$ , tool system;  $x_2y_2z_2$ , blank system;  $\varphi'_1$ , tool rotation angle;  $\varphi'_2$ , blank rotation angle

A direct solid CAD method can be used to simulate the machining [37]. In such a simulation, the model of the tool and workpiece creates discrete rotational movements resulting from the kinematics of the gear generation, and in each of the subsequent positions from the solid representing the workpiece, the

solid, being the interference with the tool and the workpiece, is subtracted. Unfortunately, owing to the complex geometry of the worm in the current CAD systems, a simulation error occurs during a machining simulation, which stops the simulation.

Therefore, a different modelling method was used. The formation of a single tooth gap was considered. By adopting the principle of relative movements, the model of the workpiece during the simulation is fixed, and all relative movements are performed by the tool. The reference model of the tool is placed in a fixed location in space and copied to the next positions resulting from the kinematics of the machining. This allows eliminating the simulation errors associated with the iterative change in the rotation angle [37]. Fig. 22 shows the starting and end positions of the tool. For the considered tooth to be properly formed, the tool must enter from the outer position into and out of the gap completely. Owing to the iterative process of the simulation, it is appropriate to automate the process through the programming of macros in a CAD environment (Fig. 23).

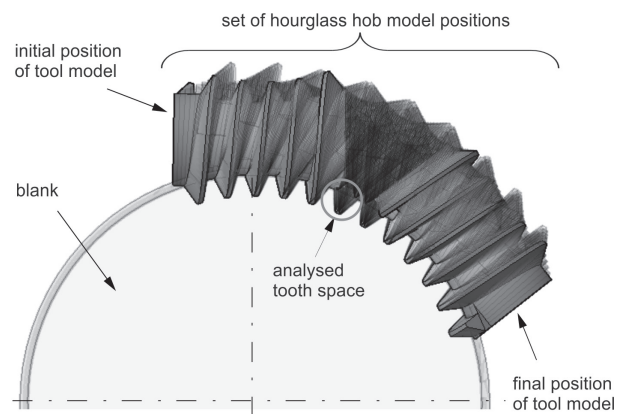


Fig. 22. Positions of the hob cutter model

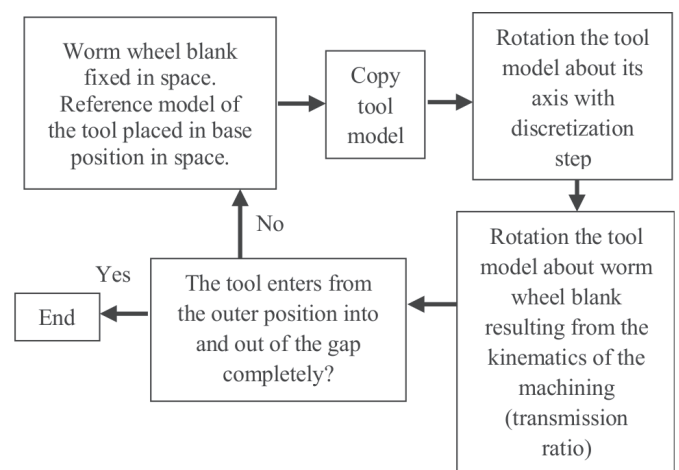


Fig. 23. Flowchart of macro simulating relative movements of the tool

Because of the simulation, a geometrical set of iterative positions of the tool relative to the workpiece is obtained (Fig. 22). The Boolean sum of this set in the worm wheel creates an object corresponding to the geometrically considered tooth space.

In addition, in this case, obtaining the sum of the Boolean set encounters problems in a CAD environment. Some iterative positions cannot be added to the rest of the model.

The tooth space of the worm wheel was determined using an indirect method. An auxiliary ring model limited by the surface of the root form, throat form, and width of the worm wheel was made (Fig. 24a). The previously obtained set of consecutive tool positions and the ring model are intersected with a set of parallel planes perpendicular to the axis of the worm wheel. This set is placed on the width of the gear (Fig. 24b). The number of sections made (the distance between them) affects the modelling accuracy of the tooth space. The sectioning operation can also be automated through macro programming (Fig. 25).

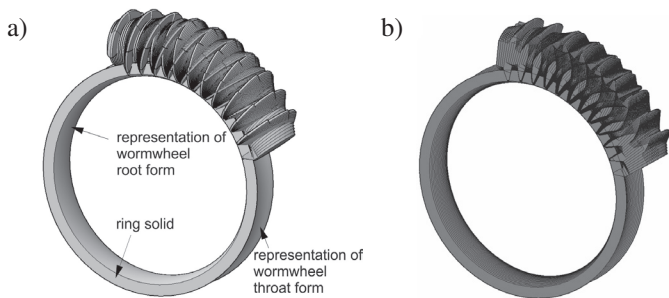


Fig. 24. Indirect method for determining the tooth space: (a) solid ring and (b) example sections

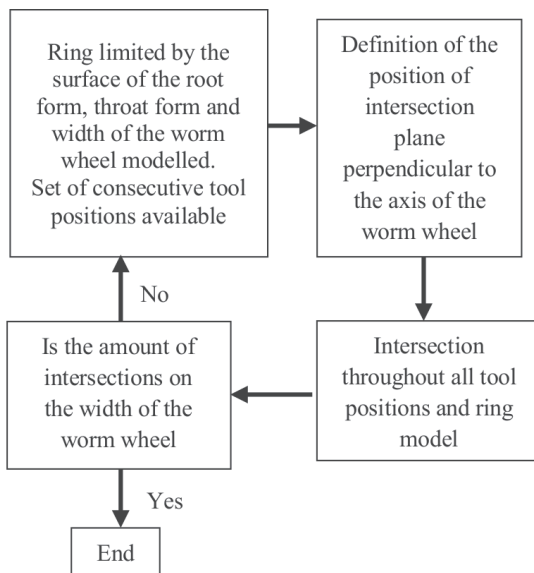


Fig. 25. Flowchart of macro for sectioning operation of the ring and set of consecutive tool positions

In each of the section planes, the outline of the analysed tooth space is separated (Fig. 26). Lines 1 and 2 in Fig. 26 are the outer envelopes of all sections of tools in the tooth space considered.

The described step should be repeated for all generated sections. A set of sections of the modelled tooth space is obtained as a frame model (Fig. 27).

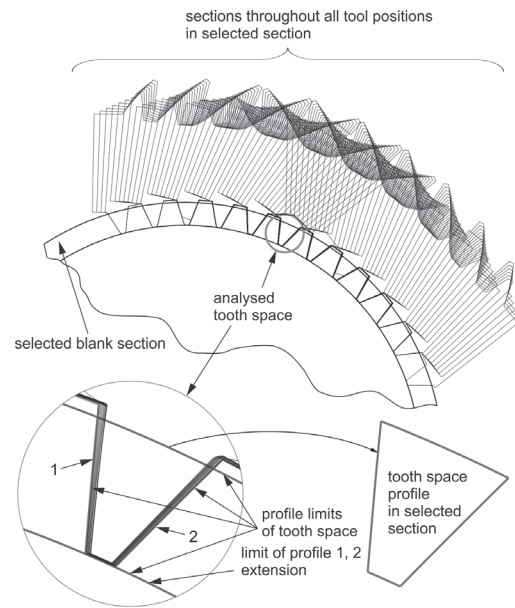


Fig. 26. Preparation of the tooth space outlines in the example section (here in the central plane)

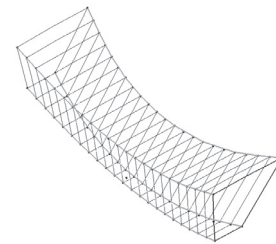


Fig. 27. Frame model of tooth space of worm wheel

Multi-section surfaces are modelled on the frame model of the tooth space (Fig. 28).

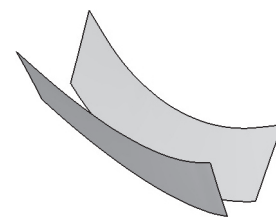


Fig. 28. Flank surfaces of the tooth space

It should be noted that the worm wheel flank is divided into three regions. Region II is an envelope of the family of contact lines of the globoid worm gear. Regions I and III are formed using the first cutting edge of the worm hob cutter [4, 17, 26]. One extreme cutting edge of the tool forms one side of the worm wheel tooth and the second edge forms the other flank. Therefore, it is necessary to determine the surface on which the edge of the tool moves during the machining of the worm wheel tooth space. The tool is in the initial position, as shown in Fig. 21. A simulation of the discrete movements of the tool and workpiece is conducted. The angle of rotation for the tool  $\varphi'_1$  is assumed such that the cutting edge at two extreme positions is

outside the blank of the worm wheel. The number of profiles depends on the discretization step, based upon which surface of the worm wheel tooth flank generated during machining is determined by the extreme edge of the tool. The discretization step should be small. At each position of the system, the extreme edge should be projected. The projected edges move with the blank. Analogously, the surface generated by the second cutting edge is then determined.

Figure 29 shows a model of a worm wheel developed based on the tooth space from Fig. 28, a tool, and a surface defined by successive positions of the extreme cutting edge. It can be seen that the part of the tooth side of the worm wheel generated using the machining simulation in a CAD environment is cut using the extreme edge of the tool (Fig. 29).

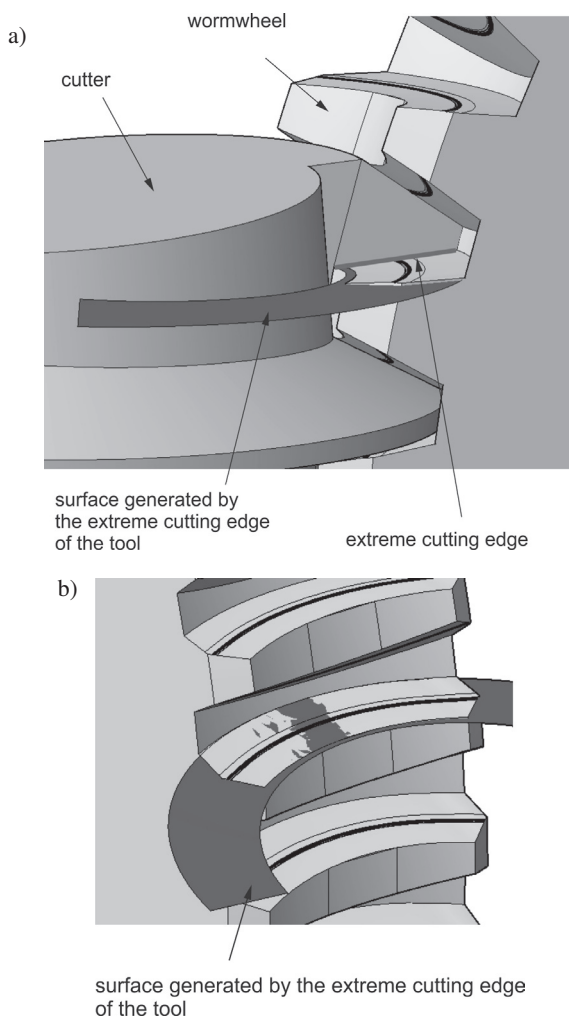


Fig. 29. Surface generated by the extreme cutting edge of the tool

New flank surfaces of the tooth space are applied, as shown in Fig. 28. There is a common part for the given surfaces (two curves for one flank). These curves are the boundaries of the regions. From the division obtained, regions I and III, as shown in Fig. 30a, and region II, as shown in Fig. 30b, are selected. The surfaces of regions I and III are connected to region II (Fig. 30c). The bottomland is made and then connected to the flank surfaces, resulting in the final tooth space model (Fig. 31).

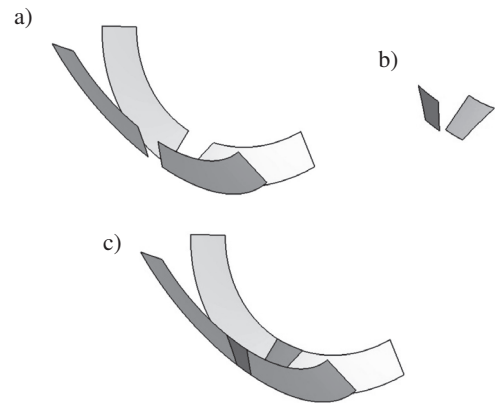


Fig. 30. Surfaces of the worm wheel tooth space: (a) defined by the extreme cutting edge (regions I and III); (b) determined using the enveloping the tool (region II); and (c) the connection of regions

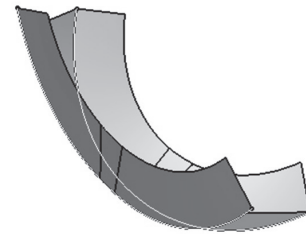


Fig. 31. Surfaces of worm wheel tooth space

The next step is to apply the surfaces of the tooth space to the worm wheel blank (Fig. 32).

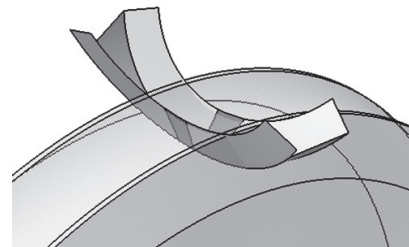


Fig. 32. Surfaces of the tooth space with the worm wheel blank

The tooth space surfaces are copied in a circular pattern. All gaps are then subtracted from the solid representing the workpiece (Fig. 33). The extreme cutting edges of the tool have a significant influence on the shape of the worm wheel flanks.

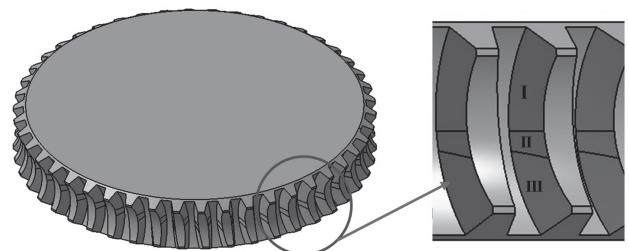


Fig. 33. Model of worm wheel with separate details and marked regions of the tooth flank

## Double enveloping worm gear modelling using CAD environment

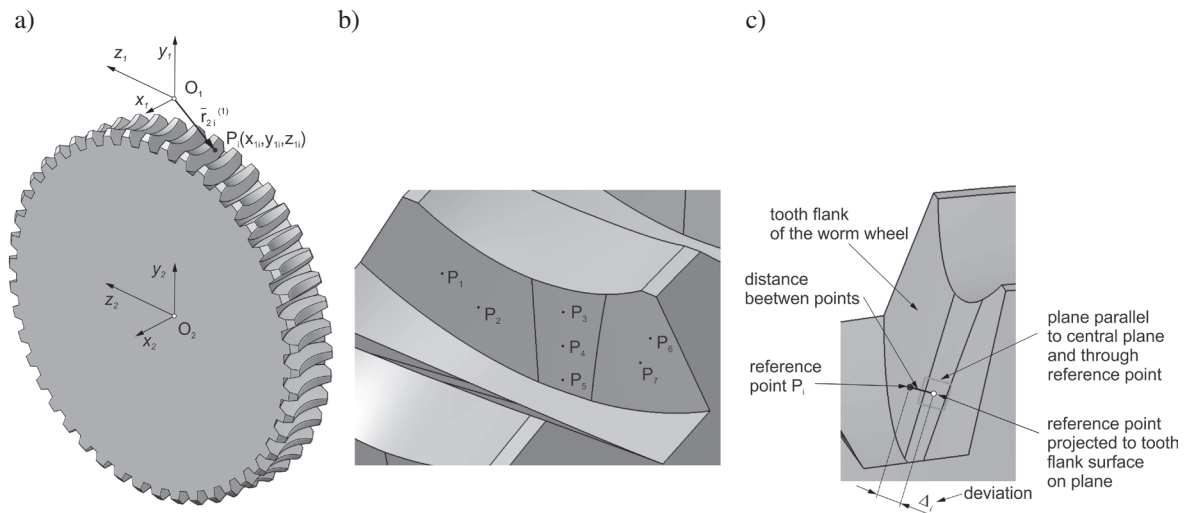


Fig. 34. Accuracy analysis of CAD model of the worm wheel: (a) coordinate system:  $\vec{r}_{2i}^{(1)}$ , element of the position vector of the worm wheel described in the coordinate system of  $x_1y_1z_1$ ;  $P_i(x_{1i}y_{1i}z_{1i})$ , reference point; (b) selected reference points; (c) determination of deviation  $\Delta$

The accuracy of the CAD model of the worm wheel was estimated by comparison with some coordinates selected from a numerical representation of the worm wheel flank surface. It was obtained according to the procedure described in [17]. The geometry of the tooth flank of the machining worm in both cases, the modelling flank surface in a CAD system, and the mathematical model, was established in the same manner. The coordinates of selected points (Table 1) were introduced into a CAD environment (Fig. 34a and b). The shortest distance between the reference point and worm wheel flank surface was determined as the distance between this point and its projection on the plane parallel to the central plane and through this reference point (Fig. 34c). The distance  $\Delta$  determines the accuracy of the CAD model. The results are presented in Table 2.

Table 1  
Reference points from a numerical model of the worm wheel flank surface

Point $P_i$	Coordinates		
	$x_1$	$y_1$	$z_1$
$P_1$	12.14343412841	-45.67253986882	-62.3985007305
$P_2$	7.548386664807	-47.86964187523	-62.0513923783
$P_3$	-3.91476606728	-43.87767864731	-61.15768739376
$P_4$	-3.620680525997	-47.95702792369	-61.25718078848
$P_5$	-3.366046488614	-52.01559524239	-61.34196141254
$P_6$	-15.59083244443	-42.37325210445	-60.31241915492
$P_7$	-14.10772668624	-45.75061160614	-60.53787834617

The worm wheel model created in a CAD system shows deviations from the mathematical model. These deviations do not exceed the value of 5 microns. Such accuracy of CAD models is sufficient in industrial practice and can be increased if needed.

Table 2  
Values of deviations

	Reference points						
	$P_1$	$P_2$	$P_3$	$P_4$	$P_5$	$P_6$	$P_7$
Deviation $\Delta$ [mm]	0.002	0.002	0.005	0.005	0.005	0.002	0.002

#### 4. Conclusions

The methodology for the modelling of members of a double enveloping worm gear in a CAD environment was presented. A method for generating a globoid helix which is the basis for modelling the worm was also described. A set of points generated in an external program were used, based upon which spline curves can be created. It is supposed that the manner of forming the end of the worm thread may have a significant effect on the stiffness and distribution of stresses in this area. It needs to be investigated in the future. Trimming a thread may result in concentrated stress at the beginning of the tooth when entering the mesh and a breaking of the tooth in this area. Additionally, a method for geometrically modifying the tooth trace was developed. A globoid worm with a tooth trace modification at the end of the thread should be characterised by more favourable stress distribution, a smoother entry into the mesh, and greater stiffness at the beginning of the thread. When modelling the worm wheel in a CAD system, it was found that owing to the complex geometry of the machining worm, simulation errors appear that prevent the use of a direct solid CAD method in generating the model. The machining of a single tooth space of the worm wheel (hybrid method) should be considered.

The presented methodology for modelling the worm gear sets in a CAD environment can be particularly useful for engineers designing such gears.

The CAD model of the globoid worm considers the whole thread length, which allows a complete analysis of the correctness of meshing. In this paper, the formation of a worm tooth beyond this range for both the active and passive tooth flank is described. The first step of the proposed solution is to cut the tooth, where the effective worm length ends. The second step is to modify the tooth trace. A globoid worm with a tooth trace modification at the ends of the thread should be characterised by more favourable stress distribution during the entry into the meshing and greater rigidity of the beginning of the thread. If the worm or worm wheel is incorrectly designed in terms of geometry, the meshing simulation of CAD models can indicate the collision.

The worm wheel model created in a CAD system shows deviations from the mathematical model. The accuracy of the CAD model of the worm wheel was estimated by comparison with some coordinates selected from a numerical representation of the worm wheel flank surface. These deviations do not exceed the value of 5 microns. Such accuracy of CAD models is sufficient in industrial practice and can be increased if needed.

CAD models are applied in the analysis of the geometrical contact pattern in a CAD environment and FEM analysis. They are nominal models for manufacturing or prototyping through the technique of rapid prototyping. They can be also used as master models for measurement, e.g. in optical technics.

## REFERENCES

- [1] I. Dudas, *The theory and practice of worm gear drives*, Penton Press, London, 2000.
- [2] W.P. Crosher, *Design and Application of the Worm Gear*, ASME Press, New York, 2002.
- [3] F.L. Litvin, *Development of Gear Technology and Theory of Gearing*, NASA, Lewis Research Center, 1999.
- [4] F.L. Litvin and A. Fuentes, *Gear Geometry and Applied Theory*, Cambridge University Press, 2004.
- [5] L. Dudás, “New technology for manufacturing quasi-globoid worm gearings”, *Mater. Sci. Eng.* 448, 012035 (2018).
- [6] Y. Chen, Y. Chen, W. Luo, and G. Zhang, “Development and Classification of Worm Drive”, *The 14th IFToMM World Congress in Taiwan*, 2015.
- [7] V. Simon, “Double Enveloping Worm Gear Drive with Smooth Gear Tooth Surface”, in *Proc. Int. Conf. on Gearing*, Zhengzhou, China, 1988, pp. 191–194.
- [8] V. Simon, “A New Type of Ground Double Enveloping Worm Gear Drive”, in *Proc. ASME 5th Int. Power Transm. and Gearing Conf.*, Chicago, 1989, pp.281–288.
- [9] V. Simon, “Load Distribution in Double Enveloping Worm Gears”, *J. Mech. Des.* 115, 496–501 (1993).
- [10] V. Simon, “Characteristics of a Modified Double Enveloping Worm Gear Drive”, in *Proc. 6th Int. Power Transm. and Gearing Conf.*, Scottsdale, 1992, pp. 73–79.
- [11] Y. Zhao and Y. Zhang, “Novel methods for curvature analysis and their application to TA worm”, *Mech. Mach. Theory.* 97, 155–170 (2016).
- [12] Y. Zhao and Y. Zhang, “Computing method for induced curvature parameters based on normal vector of instantaneous contact line and its application to Hindley worm pair”. *Adv. Mech. Eng.* 9, 168781401772188 (2017).
- [13] Y. Zhao, “Meshing analysis for TA worm”, *Mech. Mach. Sci.* 43, 13–20, (2016)
- [14] Ch. Huai and Y. Zhao, “Variable height modification of TA worm drive”, in *Proc. Inst. Mech. Eng. Part C: J. Mech. Eng. Sci.* 233, 095440621875726 (2018).
- [15] Y. Zhao, “Edge Tooth Addendum Thickness of Hindley Worm”, *Mech. Mach. Sci.* 46, 117–124 (2016).
- [16] Y. Zhao, Ch. Huai, and Y. Zhang, “Compound Modification of Globoidal Worm Drive with Variable Parameters”, *Appl. Math. Model.* 50, 17–38 (2017).
- [17] P. Polowniak and M. Sobolak, “Mathematical description of tooth flank surface of globoidal worm gear with straight axial tooth profile”, *Open Eng.* 7, 407–415 (2017).
- [18] Q. Wen, H. Xu, and W. Tang, “The Research and Analysis of the New Modification Theory of Toroidal Worm-Gearing”, *Int. Conf. Syst. Sci., Eng. Des. Manuf. Informatiz. (ICSEM)* 11, 59–62 (2010).
- [19] Y. Chen, W. Luo, Y. Chen, and G. Zhang, “Study on the spur involute gear meshing with planar enveloping hourglass worm based on local conjugate”, *Proc. Inst. Mech. Eng. Part C: J. Mech. Eng. Sci.* 232, 095440621770821 (2017).
- [20] F. He, Z. Shi, and B. Yu, “Effects of tooth surface modification on planar double-enveloping hourglass worm gear drives”, *J. Adv. Mech. Des. Syst. Manuf.* 12, JAMDSM0040-JAMDSM0040, (2018).
- [21] W. Xu, D. Qin, and W. Shi, “Direct digital design and simulation of meshing in worm-gear drive”, *Chin. J. Mech. Eng.* 19, 428–433 (2006).
- [22] L.V. Mohan and M.S. Shunmugam, “Geometrical aspects of double enveloping worm gear drive”, *Mech. Mach. Theory.* 44, 2053–2065 (2009).
- [23] K.Y. Chen and Ch.B. Tsay, “Mathematical model and worm wheel tooth working surfaces of the ZN-type hourglass worm gear set”, *Mech. Mach. Theory.* 44, 1701–1712 (2009).
- [24] Ch. Rui, H. Li, J. Yang, W. Wei, “Research on a method for designing land surfaces of a dual-cone double enveloping hourglass worm wheel hob”, *J. Adv. Mech. Des. Syst. Manuf.* 12, JAMDSM0090-JAMDSM0090 (2018).
- [25] J. Yang, H. Li, Ch. Rui, W. Wei, and X. Dong, “A Method to Generate the Spiral Flutes of an Hourglass Worm Gear Hob”, *J. Mech. Des.* 140, 063301 (2018).
- [26] Ch. Rui, H. Li, J. Yang, W. Wei, and X. Dong, “A design and generating method for grinding relief surfaces of a dual-cone double enveloping hourglass worm gear hob”, *J. Mech. Des.* 140, 123301–1 (2018).
- [27] Z. Lei, Q. Bi, Y. Wang, and H. Ding, “Five-Axis Flank Milling Method of Plane Double Enveloping Hourglass Worm”, *Adv. Mat. Res.* 314–316, 1523–1532 (2011).
- [28] S. Lagutin, E. Gudov, and B. Fedotov, “Manufacturing and load rating of modified globoid gears”, *Balkan J. Mech. Transm. (BJMT)*. 1, 45–53 (2011).
- [29] Sutyagin, L. Mal’ko, and I. Trifanov, “More efficient machining of globoid worm gears”, *Rus. Eng. Res.* 35, 623–627 (2015).
- [30] L. Dong, J. Wang, P. Liu, W. Wei, and H. Li, “An NC rough turning method of an enveloping toroidal worm”, *Prod. Eng.* 6, 129–135 (2012).
- [31] Y. Sun, H. Zheng, Q. Bi, and S. Wang, “Method of accurate grinding for single enveloping TI worm”, *Sci. China-technol. Sci.* 48, 430–440 (2005).
- [32] Z. Liu, H. Lu, G. Yu, and S. Wang, “A novel CNC machining method for enveloping surface”, *Int. J. Adv. Manuf. Technol.* 85, 779–790 (2015).

## Double enveloping worm gear modelling using CAD environment

- [33] Z. Liu, H. Lu, S. Wang, and G. Yu, "Digitization modelling and CNC machining for cone-generated double-enveloping worm drive", *Int. J. Adv. Manuf. Technol.* 95, 3393–3412 (2018).
- [34] H. Lu, Z. Liu, and S. Wang, "Digitization modelling and CNC machining for enveloping surface parts", *Int. J. Adv. Manuf. Technol.* 73, 209–227 (2014).
- [35] A.L. Kheyfets, "Geometrically Accurate Computer 3D Models of Gear Drives and Hob Cutters", *Procedia Eng.* 150, 1098–1106 (2016).
- [36] A.L. Kheyfets, "Programming While Construction of Engineering 3D Models of Complex Geometry", *Mat. Sci. Eng.* 262, 012111 (2017).
- [37] M. Sobolak, *Analysis and synthesis of mating gear tooth surface by discrete methods*, Rzeszow University of Technol. Publ., Rzeszow, 2006, [in Polish].
- [38] A.J. Muminovic, M. Colic, E. Mesic, and I. Saric, "Innovative design of spur gear tooth with infill structure", *Bull. Pol. Acad. Sci. Tech. Sci.* 68(3), 477–483 (2020).
- [39] W. Ostapski and I. Mukha, "Stress state analysis of harmonic drive elements by FEM", *Bull. Pol. Acad. Sci. Tech. Sci.* 55(1), 115–123 (2007).
- [40] M. Batsch, "Mathematical model and tooth contact analysis of convexo-concave helical bevel Novikov gear mesh", *Mech. Mach. Theory* 149, 103842 (2020).
- [41] M. Batsch, T. Markowski, S. Legutko, and G.M. Krolczyk, "Measurement and mathematical model of convexo-concave Novikov gear mesh", *Measurement* 125, 516–525 (2018).
- [42] M. Sobolak, P. Polowniak, M. Cieplak, M. Oleksy, and K. Bulanda, "Application of polymeric materials for obtaining gears with involute and sinusoidal profile", *Polimery* 7–8, 563–567 (2020).
- [43] AGMA 6135–A02, Design, Rating and Application of Industrial Globoidal Wormgearing (Metric Edition), Am. Natl. Stand., 2002.
- [44] GOST 16502–83, Basic requirements for interchange ability. Globoid gears. Tolerances, 1983.
- [45] GOST 17696–89, Globoid gears. Calculation of geometry, 1989.
- [46] GOST 24438–80, Globoid gears. Basic worm and basic generating worm, 1980.
- [47] GOST 9369–77, Globoid gear pairs. Basic parameters, 1977.
- [48] M. Sobolak, P. Polowniak, P.E. Jagielowicz, "Generating of globoid helix in CATIA environment using laws", *Mechanik* 7, 632–633 (2016), [in Polish].